Hox genes maintain critical roles in the adult skeleton

Jane Y. Song[a], Kyriel M. Pineault[b], Jesús M. Dones[c], Ronald T. Raines[c], and Deneen M. Wellik[b,1]

[a]Cellular and Molecular Biology Program, University of Michigan, Ann Arbor, MI 48109; [b]Department of Cell and Regenerative Biology, University of Wisconsin-Madison, Madison, WI 53705; and [c]Department of Chemistry, Massachusetts Institute of Technology, Cambridge, MA 02139

Edited by Denis Duboule, University of Geneva, Geneva 4, Switzerland, and approved February 11, 2020 (received for review December 2, 2019)

***Hox* genes are indispensable for the proper patterning of the skeletal morphology of the axial and appendicular skeleton during embryonic development. Recently, it has been demonstrated that *Hox* expression continues from embryonic stages through postnatal and adult stages exclusively in a skeletal stem cell population. However, whether *Hox* genes continue to function after development has not been rigorously investigated. We generated a *Hoxd11* conditional allele and induced genetic deletion at adult stages to show that *Hox11* genes play critical roles in skeletal homeostasis of the forelimb zeugopod (radius and ulna). Conditional loss of *Hox11* function at adult stages leads to replacement of normal lamellar bone with an abnormal woven bone-like matrix of highly disorganized collagen fibers. Examining the lineage from the *Hox*-expressing mutant cells demonstrates no loss of stem cell population. Differentiation in the osteoblast lineage initiates with Runx2 expression, which is observed similarly in mutants and controls. With loss of Hox11 function, however, osteoblasts fail to mature, with no progression to osteopontin or osteocalcin expression. Osteocyte-like cells become embedded within the abnormal bony matrix, but they completely lack dendrites, as well as the characteristic lacuno-canalicular network, and do not express SOST. Together, our studies show that *Hox11* genes continuously function in the adult skeleton in a region-specific manner by regulating differentiation of *Hox*-expressing skeletal stem cells into the osteolineage.**

Hox genes | skeletal homeostasis | MSCs | osteolineage differentiation | bone matrix

Hox genes are important transcription factors responsible for establishing vertebral axial morphology along the anteroposterior (AP) axis during embryogenesis (1). Additionally, the *Hox9-Hox13* paralogs are indispensable for development of the proximodistal (PD) axis of the limb (2–5). The *Hox11* paralogous group, *Hoxa11*, *Hoxc11* and *Hoxd11*, regulate the patterning of the sacral region of the vertebral column and the zeugopod skeleton of the forelimb and hindlimb (radius/ulna, tibia/fibula) (4, 5). *Hox* paralogous genes functionally compensate for one another in skeletal patterning, and all paralogs expressed in a region need to be removed for defects to fully manifest. In the forelimb, only the *Hoxa11* and *Hoxd11* paralogs are expressed; thus, the removal of these two genes leads to a severe malformation of the zeugopod skeletal elements (4, 5).

A Hoxa11eGFP knock-in reporter allele shows that Hox expression initiates broadly at embryonic day (E) ~9.5 within the developing limb bud mesenchyme but very quickly becomes restricted to the zeugopod region (6, 7). While previous work has focused largely on the embryonic role of *Hox* genes, we observed that expression is continuous in the skeleton and extends beyond development into postnatal and adult stages (7–11). Importantly, *Hox* expression remains regionally restricted and maintains the expression pattern that has been established during development (9, 12, 13). Conditional adult loss-of-function has not been examined, but *Hox11* compound mutants (animals in which three of the four paralogs are mutated) appear nearly normal at birth but begin to exhibit significant skeletal growth phenotypes at postnatal stages and are not able to enact proper fracture repair at adult stages, consistent with potential continuing functions (8–10). The interpretation of this phenotype is complicated by the fact that three of the four alleles are absent throughout embryonic development, making it impossible to separate embryonic defects that manifest later in life from continued function at adult stages.

We previously demonstrated that *Hox11* expression in the skeleton is exclusively restricted to a population of regional, progenitor-enriched mesenchymal stem/stromal cells (MSCs) (9, 11). Using a *Hoxa11-CreER^{T2}* lineage-tracing system, we recently established that the *Hox11* lineage contributes to the development, growth, and homeostasis of the zeugopod skeleton by giving rise to all of the mesenchymal lineages in the bone—osteoblasts, osteocytes, chondrocytes, and bone marrow adipocytes. Notably, this *Hox11*-expressing cell population is also maintained as self-renewing adult stem cells throughout life, demonstrating that *Hox*-expressing cells are bona fide skeletal stem cells (SSCs), continuously supplying the progenitors for bone maintenance and repair throughout the life of the animal (11).

While these previous studies have provided rigorous information on *Hox* lineage, they have not addressed whether *Hox* function is required at later stages. This study sought to examine whether *Hox* genes continue to function in the adult skeleton within the skeletal stem cell population. In order to interrogate this potential, we generated a conditional *Hoxd11* allele that, when combined with a *Hoxa11* null allele, allows us to completely delete *Hox11* function at any stage. We find that deleting *Hox11* function at adult stages results in a progressive and dramatic remodeling of the forelimb zeugopod skeleton. Using our *Hoxa11-CreER^{T2}* allele to simultaneously delete *Hox11* function and lineage-label *Hox11* mutant cells, we establish that the phenotype spatiotemporally correlates with the initiation of *Hoxd11* deletion. Adult conditional mutants accumulate a woven bone-like matrix with disorganized collagen that progressively replaces normal

Significance

Mammalian *Hox* genes are absolutely critical for proper development of skeletal morphology during embryogenesis, and *Hox11* genes are essential for proper zeugopod (radius/ulna, tibia/fibula) development. While the expression of *Hox* genes continues through postnatal and adult stages, whether *Hox* genes continue to function in the skeleton after the establishment of skeletal morphology has not been determined due to lack of genetic tools. To address this issue, we generated a conditional *Hoxd11* allele that allows for temporal deletion of *Hox11* function at adult stages following normal zeugopod development and growth of the skeleton. Here, we show that *Hox* genes function in the adult skeleton by regulating the differentiation of skeletal stem cells into the osteolineage.

Author contributions: J.Y.S. and D.M.W. designed research; J.Y.S. performed research; K.M.P., J.M.D., and R.T.R. contributed new reagents/analytic tools; J.Y.S. and D.M.W. analyzed data; and J.Y.S. wrote the paper.

The authors declare no competing interest.

This article is a PNAS Direct Submission.

[1]To whom correspondence may be addressed. Email: wellik@wisc.edu.

This article contains supporting information online at https://www.pnas.org/lookup/suppl/doi:10.1073/pnas.1920860117/-/DCSupplemental.

First published March 13, 2020.

lamellar bone. Further, we find that the *Hox11* conditional mutant animals generate preosteoblasts, but osteoblasts and osteocytes do not mature. We establish that *Hox* genes do not function solely as embryonic patterning factors in the skeleton but continue to play an important role throughout life in the skeleton.

Results

Regional Adult Hoxa11-Expressing Skeletal Stem Cells Continuously Contribute to the Adult Zeugopod Skeleton. During development, Hox11 expression is restricted to the zeugopod region where it is observed in the perichondrium region surrounding the developing cartilage anlage (7). Hox11 expression continues in cells present in the perichondrium/periosteum as the skeleton develops, also becoming visible on the endosteal bone surface and trabecular bone surface, as well as in bone marrow stromal cells as the bone marrow space is created during late embryogenesis (9, 11). This expression pattern is then maintained throughout life (9) (Fig. 1 *A*, *Inset*). Our previous work demonstrated that embryonic and postnatal *Hox11*-expressing cells are regionally restricted skeletal stem cells and that this lineage provides progenitors for all skeletal mesenchymal lineages, as well as exhibits continuous self-renewal as stem cells throughout life (11). As expected, this lineage and behavior are recapitulated when lineage labeling is initiated at adult stages. By initiating lineage labeling at adult stages in *Hoxa11-CreER^{T2};ROSA-LSL-tdTomato* animals, we show downstream lineage cells become osteoblasts on the trabecular as well as endosteal bone surfaces, and sclerostin-expressing osteocytes embedded within the cortical bone (Fig. 1 *B* and *C* and *SI Appendix*, Fig. S1 *A* and *B*).

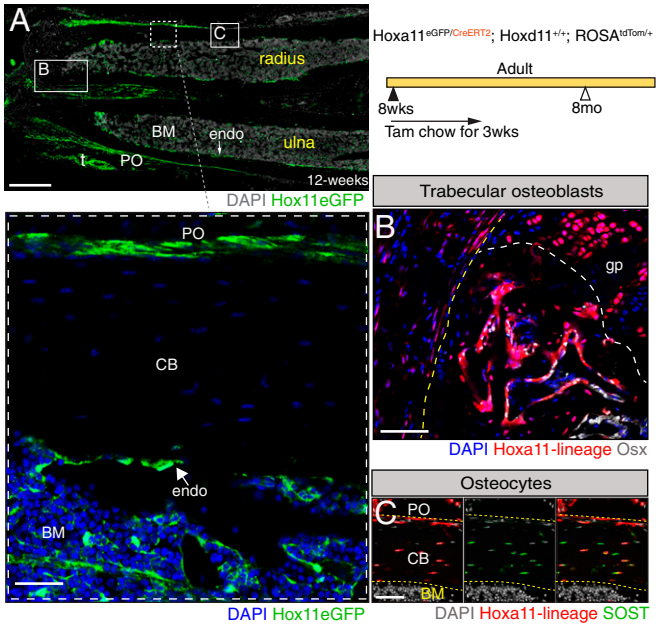

Fig. 1. Adult Hox11-expressing skeletal stem cells continuously give rise to osteoblasts and osteocytes. (*A*) Hoxa11-eGFP real-time reporter allele demonstrates continuous expression of Hoxa11 (green) at 12 wk of age. The panel was created by stitching 17 individual 10× images. t, tendon. DAPI, gray. (Scale bar: 200 μm.) Shown is a higher magnification image of the boxed area in *A* showing localization of Hoxa11 expression (green) in the periosteum, endosteum, and bone marrow compartment. BM, bone marrow; CB, cortical bone; endo, endosteum; PO, periosteum. DAPI, blue. (Scale bar: 75 μm.) Animals of the indicated genotype were fed on tamoxifen (Tam) chow at 8 to 10 wk of age for a duration of 3 wk to induce deletion and collected at 8 mo of age. Boxes marked "B" and "C" in *A* represent the approximate locations of magnified images shown in *B* and *C*. (*B*) Hoxa11-lineage marked cells (red) are found in the trabecular bone coexpressing osterix (Osx) (white). The yellow dashed line outlines the cortical bone, and the white dashed line demarcates the growth plate border. gp, growth plate. DAPI, blue. (Scale bar: 75 μm.) (*C*) Hoxa11-lineage marked cells (red) are also found as osteocytes embedded within the cortical bone coexpressing SOST (green). Hoxa11-lineage marked cells and DAPI (gray) in the far-left, SOST (green) and DAPI (gray) in the middle, and the merged image is shown in the far-right. (Scale bar: 60 μm.) All images: BM, bone marrow; CB, cortical bone; endo, endosteum; PO, periosteum.

Cas9/CRISPR Generation and Functional Validation of a Conditional Hoxd11 Allele. To induce loss of *Hox11* function at adult stages after the normal development and growth of the zeugopod skeleton, we generated a *Hoxd11* conditional allele. As all *Hox* genes contain two exons with the DNA-binding homeodomain present in exon 2, we flanked exon 2 with loxP sites using CRISPR/Cas9-mediated gene editing (14). *Cre*-mediated removal of exon 2 is expected to lead to loss of function of *Hoxd11* (Fig. 2*A*). In brief, two guide RNAs were targeted to regions of low conservation 5′ and 3′ of *Hoxd11* exon 2, and single-stranded oligo donors were designed containing a loxP sequence and 60 base pairs (bp) of flanking homology sequence on each side for targeted insertion of LoxP sites flanking *Hoxd11* exon 2. The loxP sites were targeted sequentially to the locus to generate a *Hoxd11* conditional allele through two rounds of zygote microinjection. Targeted insertion of each loxP site was confirmed by PCR and subsequent sequencing (*SI Appendix*, Fig. S2 *A* and *B*).

The *Hoxd11* conditional allele was first assessed for deletion of the region flanked by the loxP sites. Females with the genotype *Hoxa11$^{eGFP/+}$;Hoxd11$^{loxP/loxP}$* were mated to males with the genotype *ROSA$^{CreERT2/+}$;Hoxa11$^{+/-}$;Hoxd11$^{loxP/loxP}$* to generate embryos with the genotype *ROSA$^{CreERT2/+}$;Hoxa11$^{eGFP/-}$;Hoxd11$^{loxP/loxP}$*. PCR analyses on embryonic tissue were performed, and the *Hox11* conditional mutant embryos produced a robust recombined band and an absence of a detectable control band, indicating efficient deletion (Fig. 2*B*).

To functionally validate this allele, we deleted *Hoxd11* at embryonic stages in the background of *Hoxa11*-null mutants. It is important to note that the *Hoxa11-eGFP* is a knock-in allele that renders it nonfunctional. Therefore, animals that carry the genotype *Hoxa11$^{eGFP/-}$* are functionally null for *Hoxa11*, but their forelimbs are indistinguishable from that of wild-type (WT) littermates from embryonic through adult stages, serving as a good control for the conditional mutants (compare Fig. 2 *C* and *D*) (5). We induced deletion by feeding pregnant dams tamoxifen chow for 1 wk beginning at E9.5. This stage is approximately when *Hox11* expression begins within the limb bud and therefore should recapitulate the *Hox11*-null phenotype. Embryos were collected at E17.5, and skeletal preparations demonstrate that Hox11 conditional mutants phenocopy *Hoxa11$^{-/-}$; Hoxd11$^{-/-}$* mutants, confirming that the *Hoxd11* conditional allele results in deletion of *Hoxd11* function (compare Fig. 2 *E* and *F*).

Adult Deletion of Hox11 Function Results in a Progressive Replacement of Lamellar Bone with Abnormal Bony Matrix. To assess the role of *Hox11* during adult skeletal homeostasis, animals with the genotype *ROSA$^{CreERT2/+}$;Hoxa11$^{eGFP/-}$;Hoxd11$^{loxP/loxP}$* (referred to as *Hox11^{ROSACreERT2}* conditional mutants) and corresponding controls (including animals of identical genotype minus the *ROSA26-CreER^{T2}* with tamoxifen administration, and animals with the *ROSA26-CreER^{T2}* in the absence of tamoxifen administration) were examined. Of note, there was minimal recombination in the absence of tamoxifen administration in animals with the *ROSA26-CreER^{T2}* allele; these animals did not produce a phenotype or show any evidence of recombination at the *Hoxd11* locus as assessed by PCR (*SI Appendix*, Fig. S2 *C* and *D*).

Both control and conditional mutant adult animals were fed tamoxifen chow for 3 wk beginning at 8 to 10 wk of age and evaluated at 2, 4, or 10 mo after the initiation of deletion. Tail samples were processed for PCR analysis and confirmed high levels of recombination, even out to the 1-y time point (Fig. 3*A*).

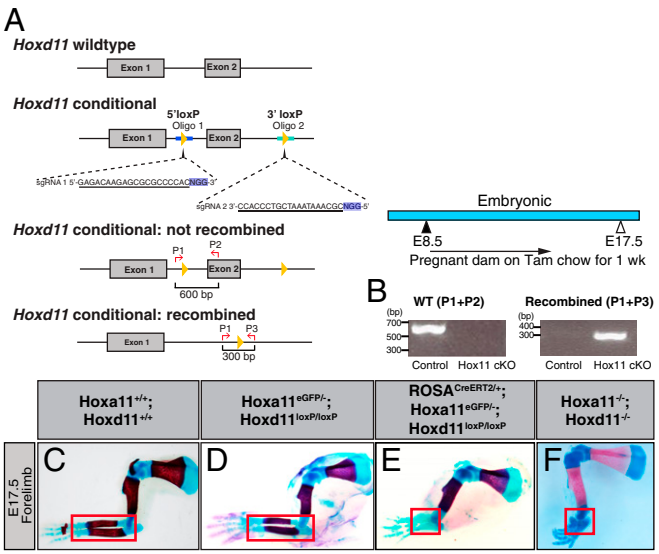

Fig. 2. Conditional deletion of Hox11 function recapitulates the germline null mutation. (*A*) Schematic illustrating the *Hoxd11* locus. Yellow arrowheads illustrate the inserted loxP sites. Two guide RNAs with the indicated sequences (underlined) along with their corresponding PAM (highlighted blue) were used to flank exon 2 of *Hoxd11* in order to insert loxP sites. Homology sequences used in the donor sequences are highlighted with thick dark blue line (5′ loxP) and thick light blue line (3′ loxP). Red arrows marked with P1, P2, and P3 mark the location of the PCR primers used to confirm recombination. Corresponding PCR product sizes are indicated as well. The PCR elongation time was adjusted so that a 300-bp PCR product would appear only if recombination had occurred between the loxP sites. Pregnant dams were fed on tamoxifen chow for 1 wk to induce recombination, and the resulting embryos were collected at E17.5. (*B*) PCR analysis using the PCR primers produces a robust 600-bp control band only present in the controls and a 300-bp recombined band only present in the conditional mutants. cKO denotes Hox11 conditional mutants. Skeletal preparations of limbs from (*C*) WT, (*D*) littermate control for Hox11 conditional mutant, (*E*) Hox11^{ROSACreERT2} conditional mutant, and (*F*) Hox11 germline-null mutant. The red box highlights the zeugopod skeleton.

Notably, recombination was measured at the same degree in tail samples as in the zeugopod skeleton (*SI Appendix*, Fig. S2*E*). A small number of the *Hox11*^{ROSACreERT2} conditional mutants displayed a residual WT band, indicating incomplete recombination; however, qRT-PCR analyses revealed robust loss of *Hoxd11* in all cases (Fig. 3*B*). Despite robust loss of function, it is critical to note that the *Hox11*-expressing skeletal stem cells are maintained in the conditional mutant bones out to the 1-y-old time points, as supported by continued *Hoxa11eGFP* expression (*SI Appendix*, Fig. S3 *A* and *B*).

Microcomputed tomography (microCT) measurements did not reveal significant distinctions between the control and *Hox11*^{ROSACreERT2} conditional mutants at any of the time points examined (*SI Appendix*, Fig. S4 *A* and *B*). However, histological inspection revealed progressive changes in the appearance of the cortical bone in *Hox11*^{ROSACreERT2} conditional mutants compared to controls. Conditional mutant bones become notably hypercellular, and quantification revealed significantly higher cell numbers in the abnormal bony matrix (Fig. 3 *C*–*I*). Presumed osteocytes embedded within the hypercellular matrix displayed a round morphology compared to the ellipsoid morphology in controls (compare Fig. 3 *D* and *G*, *Inset*). Comparing the percentage of osteocytes exhibiting an ellipsoid morphology in the lamellar bone (Fig. 3 *F*–*H*, above the dashed line) to those in the abnormal bony matrix (Fig. 3 *F*–*H*, below the dashed line, green bracket) in the *Hox11*^{ROSACreERT2} conditional mutants revealed a significant decrease in the presence of ellipsoid osteocytes in the abnormal bone matrix (Fig. 3 *F*–*H* and *J*). This phenotype resembles the histology of woven bone, which has a higher density of osteocytes within its matrix along with the round shape of the lacunae (15). It is important to note that these abnormalities remain regionally restricted as the humerus of *Hox11*^{ROSACreERT2} conditional mutants was not affected even as late as the 1-y time point (Fig. 3 *K* and *L*).

Abnormal Bony Matrix in Adult Hox11 Conditional Mutants Displays Disorganized Collagen. The shape of osteocyte lacunae is strongly influenced by the orientation of the collagen fibers within the bone. Normal adult bone is comprised of lamellar bone, with collagen fibers arranged in organized parallel sheets or layers, and this contributes to the ellipsoid shape of the lacunae (16, 17). Woven bone, in contrast, is characterized by a haphazard organization of collagen fibers and contains osteocyte lacunae with a spherical shape, similar to what is observed in the abnormal matrix of the *Hox11* conditional mutants. The collagen network within cortical bone can be visualized by picrosirius red stain. Picrosirius red increases the birefringence of the collagen fibers, and subsequent observation under polarized light reveals the organization of the collagen network (18, 19). The picrosirius red staining in control bone demonstrates a well-organized, parallel structure of collagen fibers characteristic of normal, mature lamellar bone while the *Hox11*^{ROSACreERT2} conditional mutant bones displayed a striking disorganization of the collagen matrix that correlates with the hypercellular region (Fig. 4 *A*–*F*). Notably, both the region of disorganized collagen matrix and the hypercellular region increase with increasing time after deletion (Fig. 3 and *SI Appendix*, Fig. S5 *A*–*L*).

In efforts to further examine collagen organization, a $(flpHypGly)_7$ collagen mimetic peptide (CMP) conjugated to a cyanine 5 (Cy5) dye was used to stain sections of control and *Hox11*^{ROSACreERT2} conditional mutant bone. The ^{Cy5}CMP mimics the proline-hydroxyproline-glycine amino acid triplet motif that is prevalent in collagen (constituting ∼10.5% of the protein sequence) and selectively anneals to disrupted sites in collagen (20). Control bone sections were virtually devoid of any staining, as expected for a highly organized collagen matrix, but conditional mutant bones displayed strong binding throughout the regions of abnormal matrix (Fig. 4 *G*–*J*). Use of a compositional isomer (^{Cy5}CI) control demonstrated no binding to either control or mutant bone sections (*SI Appendix*, Fig. S5 *M* and *N*) (20).

As osteoclasts have a strong influence on bone integrity, we examined osteoclast number and localization in the controls and conditional mutants. Tartrate-resistant acid phosphatase (TRAP) is a metallophosphoesterase that participates in osteoclast-mediated bone resorption and is used to visualize osteoclasts (21). In control bones, TRAP staining is concentrated along the endosteal bone surface. In the *Hox11*^{ROSACreERT2} conditional mutant bones, TRAP staining is also observed on the endosteal bone surface; however, there are trails of TRAP stain present within the abnormal cortex of the conditional mutant bones (Fig. 4 *K* and *L*). A higher magnification of the osteoclasts on the control bone surface demonstrates that the osteoclasts and TRAP stain localize at the surface of the bone as expected while conditional mutant bone additionally shows TRAP enzyme within the abnormal bone matrix (*SI Appendix*, Fig. S6 *A* and *B*). However, there were no cells associated with the TRAP stain, leading to the conclusion that the abnormal matrix is allowing diffusion of the enzyme into the matrix (*SI Appendix*, Fig. S6 *C* and *D*). As TRAP expression by osteoclasts has been shown to influence normal endochondral bone formation and bone remodeling (22, 23), it is possible that the diffusion of the TRAP enzyme into the bone matrix exacerbates the abnormal matrix phenotype observed in the Hox11 conditional mutants. While TRAP staining is expanded in the conditional mutant bones, quantification of the bone surface osteoclasts shows no significant difference in the number of osteoclasts in the control and conditional mutants (Fig. 4*M*). The disorganized collagen matrix, in conjunction with the diffusion of

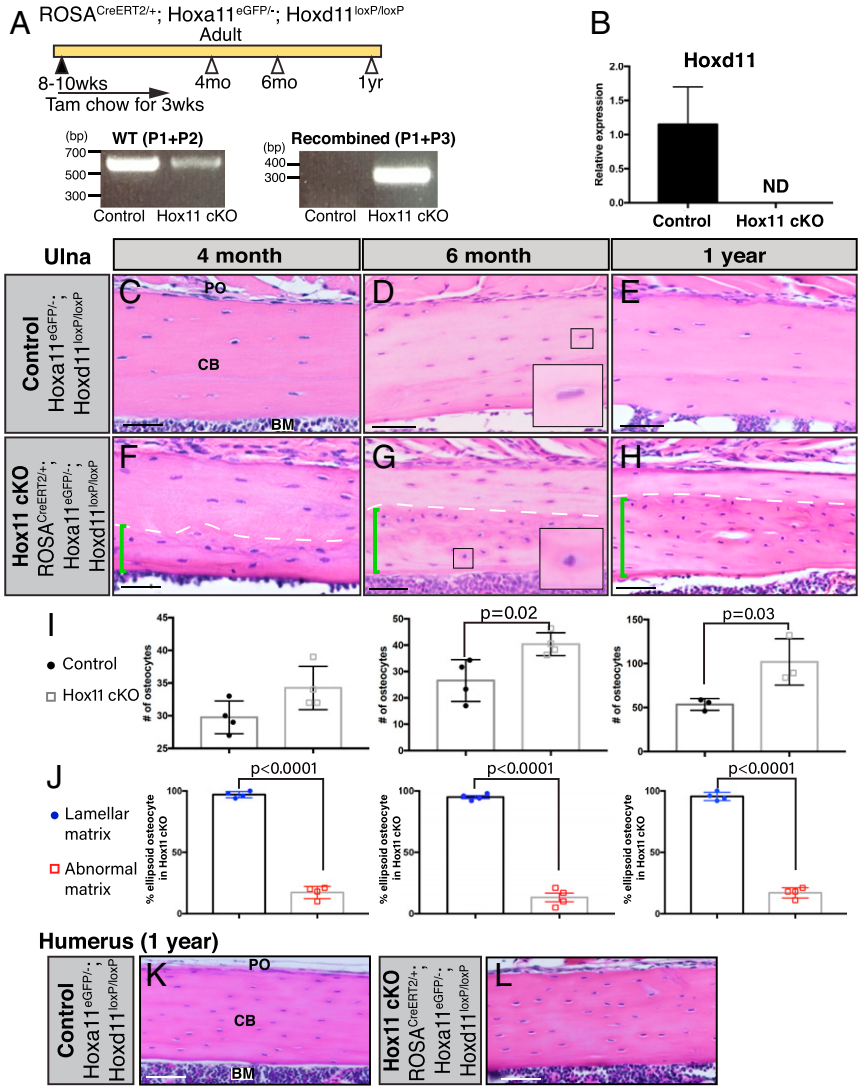

Fig. 3. Deletion of Hox11 function at adult stages results in the regional disruption in cortical bone homeostasis. Hox11 conditional mutants with the *ROSA-CreER^{T2}* (genotype indicated) allele along with control animals were fed on tamoxifen chow beginning at 8 to 10 wk of age for a total of 3 wk to delete *Hox11* function. Animals were evaluated at 4 mo of age, 6 mo of age, and 1 y of age. (*A*) Tail samples from all animals collected were analyzed via PCR to assess recombination. A robust 300-bp band in the conditional mutants demonstrates strong recombination. (*B*) qRT-PCR of Hoxa11eGFP-expressing zeugopod skeletal cells from the conditional mutants show robust deletion of *Hoxd11* in the conditional mutants. Data are presented relative to mouse GAPDH using the ΔΔCt method. ND, none detected. Error is represented as mean ± SEM. (*C–H*) H&E stains of paraffin bone sections (ulna) of control and Hox11^{ROSACreERT2}conditional mutant animals. The dashed line demarcates the border between lamellar (above) and abnormal (below) bone. Green brackets demarcate the abnormal matrix. Boxed areas in *D* and *G* represent high-magnification images of an individual matrix-embedded cell highlighting the morphological differences between control and *Hox11* conditional mutant osteocyte-like cells. (*I*) Quantification of cells embedded within the abnormal matrix at 4 mo, 6 mo, and 1 y of age shows a significant increase in cell number in Hox11^{ROSACreERT2} conditional mutant bone. Error is represented as mean ± SEM. Statistics by Student's *t* test. (*J*) Percentage of osteocytes or osteocyte-like cells in Hox11 conditional mutant bones that exhibit an ellipsoid shape within lamellar (above dotted line in *F–H*) and abnormal (below dotted line, green bracket in *F–H*) bony matrix. Error is represented as mean ± SEM. Statistics by Student's *t* test. (*K* and *L*) H&E stains of bones from the humerus of control (*K*) and Hox11 conditional mutant (*L*) show no differences in morphology at 1 y of age. All images: BM, bone marrow; CB, cortical bone; PO, periosteum. (Scale bar in all images: 100 μm.)

TRAP staining in the cortical matrices, indicates the presence of a defective matrix in the *Hox11^{ROSACreERT2}* conditional mutant bone.

Abnormal Bony Matrix Arises from Hox11-Lineage Cells. We next used the *Hoxa11-CreER^{T2}* allele to simultaneously delete the function of *Hox11* and lineage-trace the *Hox*-expressing cells by including a *ROSA26-LSL-tdTomato* allele. Females with the genotype *Hoxa11$^{eGFP/+}$;Hoxd11$^{loxP/loxP}$* were mated to males with the genotype *Hoxa11$^{CreERT2/+}$;Hoxd11$^{loxP/loxP}$;ROSA$^{LSL\text{-}tdTom/LSL\text{-}tdTom}$* to generate embryos with the genotype *Hoxa11$^{CreERT2/eGFP}$;Hoxd11$^{loxP/loxP}$;ROSA$^{LSL\text{-}tdTom/+}$* (referred to as Hox11^{Hoxa11CreERT2} conditional mutants). The genotype of the control animals for the Hox11^{Hoxa11CreERT2} conditional mutants was *Hoxa11$^{CreERT2/eGFP}$;ROSA$^{LSL\text{-}tdTom/+}$* where both the *Hoxa11-CreER^{T2}* and *Hoxa11-eGFP* are knock-in alleles rendering the *Hoxa11* alleles nonfunctional. Conditional mutant animals, along with their corresponding controls, were given tamoxifen chow for 3 wk, and the contribution of the Hox11 lineage-labeled cells to bone was examined 2 mo following the initiation of deletion. The extent of lineage contribution observed between the control and *Hox11^{Hoxa11CreERT2}* conditional mutant bones is similar, with no obvious differences in the cortical thickness of lineage-marked cells embedded in the bone matrix (Fig. 5 *A* and *B*). Control bones display a well-organized bone structure, with lineage-labeled osteocytes embedded in

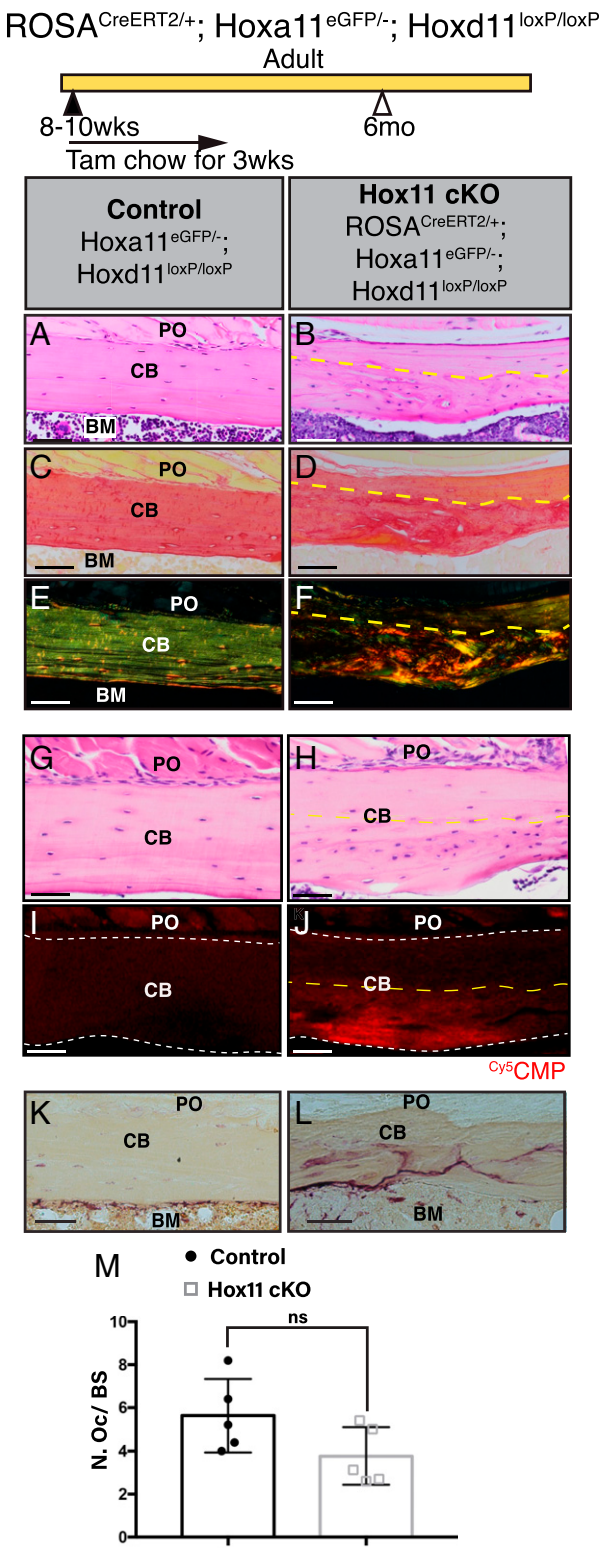

Fig. 4. Woven bone-like region in the Hox11 conditional mutant bones has a disorganized collagen matrix. Hox11 conditional mutants with the *ROSA-CreER*^{T2} (genotype indicated) allele along with control animals were fed on tamoxifen chow for 3 wk beginning at 8 to 10 wk of age to induce deletion, and animals were examined at 6 mo of age. (*A* and *B*) H&E stains of paraffin-processed bone sections of control and Hox11^{ROSACreERT2} conditional mutant animals. (*C* and *D*) Brightfield images of picrosirius red stain of consecutive bone sections from *A* and *B*. (*E* and *F*) Polarized light images of picrosirius red stain of bone sections from *C* and *D*. (*G* and *H*) H&E stains of paraffin-processed bone sections of control and Hox11^{ROSACreERT2} conditional mutant animals. (*I* and *J*) Consecutive bone sections from *G* and *H* stained with ^{Cy5}CMP (red). White dashed line marks border of cortical bone. (*K* and *L*) Control (*K*) and Hox11^{ROSACreERT2} conditional mutant (*L*) bone sections stained with TRAP. Note the distinct distribution of TRAP stain in conditional mutant. (*M*) Quantification of osteoclast number (N. Oc) on bone surface (BS) using the Bioquant Osteo software. Statistics by Student's *t* test. Error is represented as mean ± SEM. All images are from the ulna. BM, bone marrow; CB, cortical bone; PO, periosteum. The yellow dashed line demarcates border between lamellar (above) and abnormal (below) bone. ns, not significant. (Scale bar in all images: 100 μm.)

the lamellar bone (Fig. 5*A*). In contrast, the region with *Hox11*-lineage mutant cells precisely correlates with the abnormal matrix region clearly distinguishable in brightfield images (Fig. 5*B*, black bracket). These results strongly support that the abnormal matrix formed in the conditional mutant bones arises from the descendants of the cells that have lost *Hox11* function.

Hox11 Conditional Mutant Osteoblasts Exhibit Deficient Differentiation. During normal osteoblast differentiation, Runx2 marks cells that have committed to the osteoblast lineage (preosteoblasts). Maturation of osteoblasts leads to the expression of osteopontin (Opn) at relatively early stages of osteoblastic differentiation, and osteocalcin (Ocn) is expressed in fully mature osteoblasts coincident with their assuming the characteristic cuboidal shape (24). To determine whether *Hox* mutant cells initiate osteoblast differentiation, Runx2 expression was examined. Runx2 expression was observed in both control and mutant bones on the cell surface of the endosteal bone, supporting the initiation of osteoblast differentiation in both controls and mutants (Fig. 5 *C* and *D*). However, Hox11^{Hoxa11CreERT2} conditional mutant bones were almost completely devoid of both Opn and Ocn staining whereas the expression of both markers lined the endosteal surface of the control bones (Fig. 5 *E*–*H*). These data provide strong evidence that differentiation toward the osteoblast lineages is able to initiate in *Hox11* mutant skeletal stem cells, but terminal differentiation of osteoblasts is disrupted.

Morphologically, mature osteoblasts are recognizable as large cuboidal cells, with a round nucleus located in the cell away from the bone surface (25). As we have previously established that *Hox11* is not expressed in osteoblasts, but only the stem/progenitor cells, we identified probable bone surface osteoblasts as *Hoxa11eGFP*-negative, *Hoxa11* lineage-positive (red) cells. In control bones, we observed mature osteoblasts that present the classical, cuboidal morphology and nuclear localization (Fig. 5 *I*–*I*″, yellow arrowheads). Noticeably, bone surface cells that retained *Hoxa11eGFP* expression displayed a rounder morphology but were not cuboidal in shape, nor was the localization of the nucleus polarized away from the bone surface. In notable contrast to controls, all bone surface cells in conditional mutant bones appeared flatter compared to those in controls with no nuclear migration away from bone surface, consistent with loss of fully differentiated osteoblasts (Fig. 5 *J*–*J*″, yellow arrowheads).

Osteocyte Differentiation and Morphology Is Disrupted with Loss of Hox11 Function. Osteocytes are terminally differentiated osteoblasts that become embedded within the bone matrix and are the primary mechanosensory cells of the bone, with important roles in bone homeostasis (26, 27). Long dendritic processes are characteristic of osteocytes; these structures connect neighboring osteocytes to each other, as well as to bone surface, including to the cell surface osteoblasts and osteoclasts (28, 29). To examine whether osteocytes were also affected by the loss of *Hox11* function, we used a silver nitrate stain to visualize osteocyte morphology. After deletion, the Hoxa11^{CreERT2} conditional mutant matrix-embedded cells form no dendrites and display a

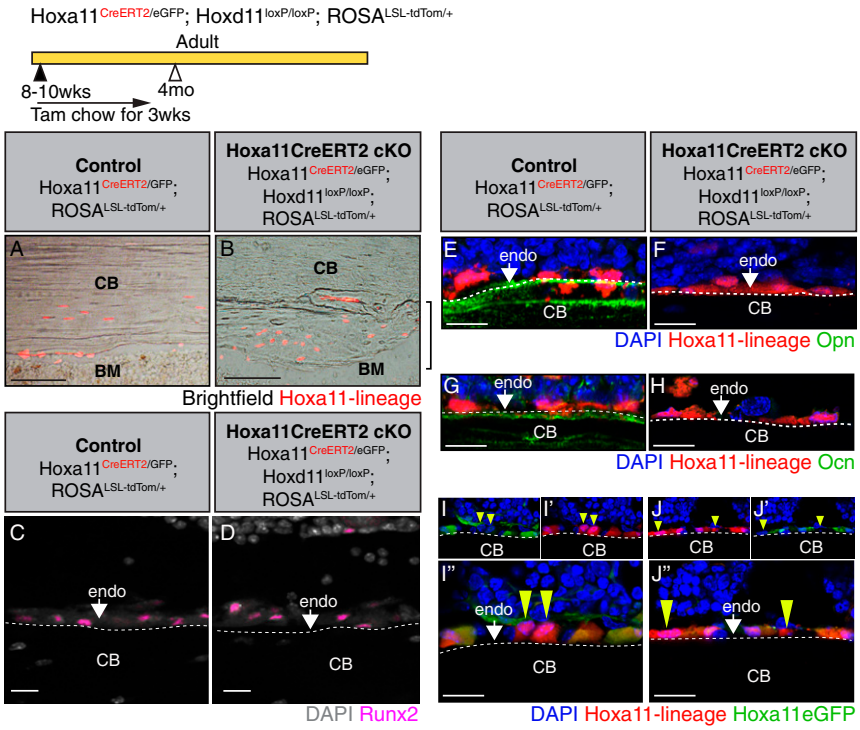

Fig. 5. Osteoblast differentiation is perturbed in Hox11 conditional mutant bone. Hox11 conditional mutants with the *Hoxa11-CreER*^{T2} allele (genotype indicated) along with control animals were fed on tamoxifen chow for 3 wk starting at 8 to 10 wk of age and collected at 4 mo of age. (*A*) Brightfield image of a bone section from a control animal overlaid with Hox11-lineage marked cells (red) shows contribution to osteocytes. (*B*) Brightfield image of bone section from a Hox11^{Hoxa11CreERT2} conditional mutant overlaid with Hox11-lineage–positive cells (red) shows contribution to abnormal bone matrix. (*C* and *D*) Control (*C*) and Hox11^{Hoxa11CreERT2} conditional mutant (*D*) bone stained with RUNX2 (magenta). DAPI, gray. White arrows in *C* and *D* mark the endosteal bone surfaces. (*E* and *F*) Control (*E*) and Hox11^{Hoxa11CreERT2} conditional mutant (*F*) bone stained with osteopontin (Opn, green). (*G* and *H*) Control (*G*) and Hox11^{Hoxa11CreERT2} conditional mutant (*H*) bone sections stained with osteocalcin (Ocn, green). (*I–J″*) Hoxa11eGFP (green) and DAPI (blue) in *I* and *J*, Hoxa11-lineage marked cells (red) and DAPI (blue) in *I′* and *J′*, and merged images in *I″* and *J″*. Control (*I–I″*) and Hox11^{Hoxa11CreERT2} conditional mutant (*J–J″*) bone sections show Hoxa11-lineage marked (red), non-Hoxa11eGFP endosteal surface osteoblasts (yellow arrowhead). Notice stark difference in morphology. All images are from the ulna. DAPI, blue (unless noted otherwise); Hox11-lineage marked cells, red. CB, cortical bone; endo, endosteum. The white dashed line demarcates the endosteal surface. (Scale bars in all images: 50 μm.)

complete absence of the normal lacuno-canalicular network within abnormal bone matrix regions.

Mature osteocytes produce and secrete the protein sclerostin, encoded by the *SOST* gene. Using our *Hoxa11-CreER*^{T2} allele with deletion enacted at 8 wk and animals evaluated 2 mo later, *Hox11*-lineage marked cells are found embedded in both the control and *Hox11*^{Hoxa11CreERT2} conditional mutant bones (Fig. 6 *E* and *F*). While virtually all of the lineage-marked osteocytes in the control bone express SOST, most *Hox11*^{Hoxa11CreERT2} conditional mutant lineage-marked, bone-embedded cells failed to express SOST (Fig. 6 *E–M*), demonstrating a requirement for *Hox* function in proper osteocyte differentiation.

Discussion

Woven bone is made primarily during the rapid bone growth of embryogenesis or following bone injury (e.g., fracture) (30, 31). In both cases, the initial woven bone matrix is remodeled and replaced by lamellar bone through a process that is not fully understood. The haphazard organization of collagen in the woven bone matrix causes the bone to be mechanically weak (32); therefore, the replacement of the woven bone matrix by lamellar bone is imperative for proper bone function and homeostasis. The accumulation of woven bone with no signs of lamellar remodeling in our *Hox11* conditional mutants demonstrates that maintaining the integrity of the skeletal matrix requires *Hox* function. All of the evidence presented in this study supports defective differentiation of osteolineage cells with the loss of *Hox11* function. Osteoblasts originate from skeletal stem cells, and previous work from our laboratory, as well as results presented here, unequivocally demonstrates that *Hox11*-expressing skeletal stem cells give rise to osteoblasts in the skeleton. As *Hox11* expression is restricted to the stem cell population and is not observed in differentiated skeletal cells, we conclude that Hox proteins function in the skeletal stem cells at early stages of differentiation.

The results from our conditional Hox11 loss-of-function model correlate with earlier investigations into embryonic null mutants. When *Hoxa11*/*Hoxd11*-null mutants were examined at E14.5, the stage at which overt osteoblasts are beginning to differentiate in the zeugopod skeletal anlage, Runx2 expression was observed in the perichondrial region (33). However, subsequent zeugopod skeletal development in the *Hoxa11*/*Hoxd11*-null mutants is grossly stunted, consistent with aberrant osteoblast differentiation. Intriguingly, these results are consistent with a similar function for Hox in the skeleton throughout life; however, this idea requires further investigation.

The abnormal collagen matrix secreted by the adult conditional mutant osteoblasts may have a compounding role in the skeletal phenotype. Mice that harbor a mutation in *Col1a1* that produces type 1 collagen molecules resistant to cleavage by collagenase manifest a haphazard endosteal bone growth reminiscent of the *Hox11* conditional mutant bones (34). The binding of ^{Cy5}CMP to collagen strands in our *Hox11* conditional mutant bone supports the presence of abnormal collagen in the matrix. The similarity in bone phenotypes suggests that the abnormal collagen matrix is a critical manifestation of the *Hox* conditional

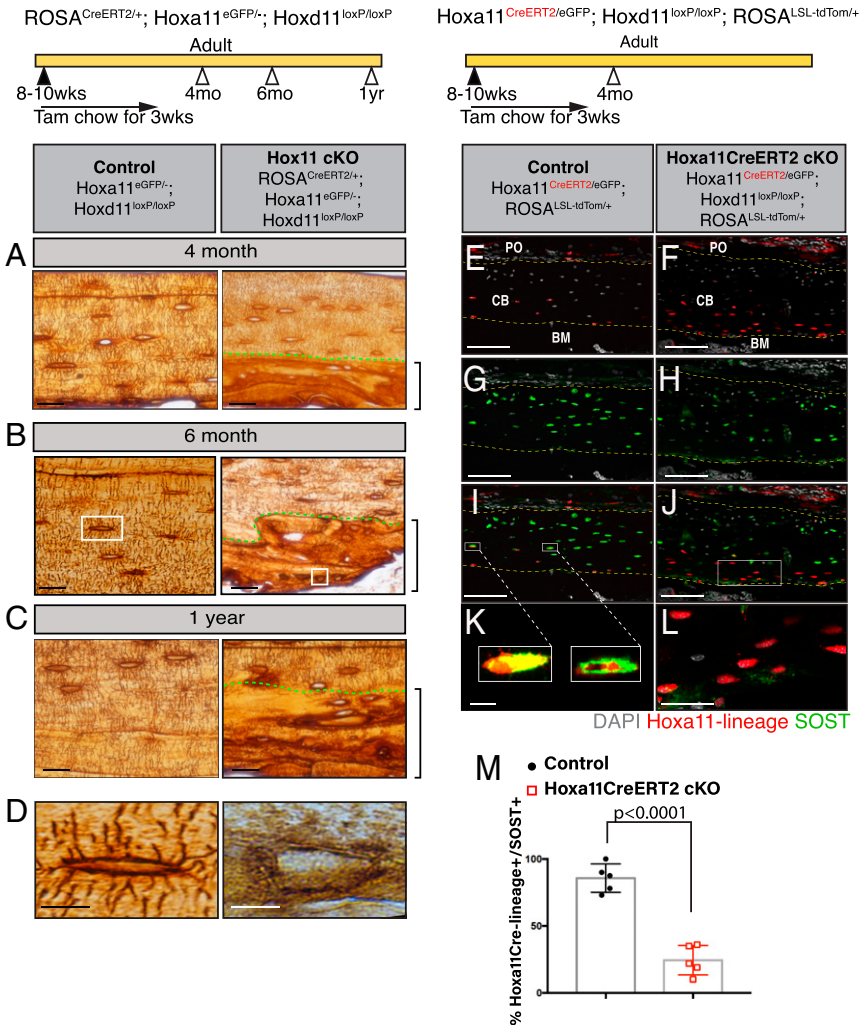

Fig. 6. Hox11 conditional mutant osteocytes fail to form dendrites or express SOST. Hox11 conditional mutants with the *ROSA-CreER^{T2}* (genotype indicated) allele along with control animals were fed on tamoxifen chow beginning at 8 to 10 wk of age for 3 wk to delete *Hox11* function, and animals were evaluated at 4 mo of age, 6 mo of age, and 1 y of age for *C–E*. (*A–C*) Control (*Left*) and Hox11^{ROSACreERT2} conditional mutants (*Right*) were treated with silver nitrate. Green dashed lines demarcate the lamellar (above) and abnormal (below) bone. Brackets outline abnormal bone matrix. (*D*) High magnification of osteocytes from the white-boxed area in *B*. Hox11 conditional mutants with the *Hoxa11-CreER^{T2}* allele (genotype indicated) along with control animals were fed on tamoxifen chow for 3 wk starting at 8 to 10 wk of age and collected at 4 mo of age for *E–M*. (*E* and *F*) Control (*E*) and Hox11^{Hoxa11CreERT2} conditional mutant (*F*) bone sections showing Hox11-lineage marked cells (red) that contributed to osteocytes. (*G* and *H*) Control (*G*) and Hox11^{Hoxa11CreERT2} conditional mutant (*H*) bone sections stained with SOST (green). (*I* and *J*) Merged images of *E* and *G* in *I* or *F* and *H* in *J* showing overlap or the lack thereof of Hox11-lineage marked cells (red) and SOST (green). The yellow dashed line in *E–J* outline the cortical bone. (*K* and *L*) Close-up of osteocytes in white-boxed region in *I* and *J*. (*M*) Quantification of Hox11-lineage marked cells (red) that also express SOST (green). Error is represented as mean ± SEM. Statistics by Student's *t* test. All images are from the ulna. DAPI, gray. BM, bone marrow; CB, cortical bone; PO, periosteum. (Scale bar: 25 μm [*A–C*], 10 μm [*D*], 100 μm [*E–J*], 10 μm [*K* and *L*].)

loss-of-function phenotype. It is possible that collagen helices produced by *Hox* mutant osteoblasts are not processed properly for the normal organization to lamellar bone, or there may be an absence of enzymes or other molecules necessary for proper remodeling of the collagen matrix. This abnormal collagen matrix may create a more permissive environment for osteoblast incorporation, leading to the apparent increase in the number of osteocyte-like cells.

Our results test a hypothesis recently put forward by Leucht and coworkers that *Hox* expression in periosteal stem/progenitor cells determines the cell fate of those stem/progenitor cells in adult animals (35). In this report, the authors associated *Hox*-expressing periosteal stem/progenitor cells with more primitive, stem cell-like gene ontology terms that exhibited more accessible chromatin at transcriptional start sites. This is consistent with recent work from our laboratory demonstrating that *Hox* expression is associated with skeletal stem cells and lineage label into downstream skeletal lineages (9, 11). Further, results presented here provide direct, genetic support for their hypothesis that *Hox* genes confer differentiation cues to these stem cells throughout life. Leucht and coworkers also hypothesize that *Hox* function may be required for maintenance of the stem cell population (35). However, we have previously shown that *Hox11*-expressing skeletal stem cells are maintained in *Hox11* compound mutants at relatively comparable numbers compared to controls (9). In this study, we precisely test complete loss of function and find that Hoxa11eGFP-positive skeletal stem cells are still present 10 mo after deletion of *Hox* function. Furthermore, the progressive nature of the phenotype observed in our *Hox11* conditional mutants supports maintenance of the *Hox11*-expressing skeletal stem population for continued (abnormal) contribution to the osteolineage. Cumulatively, these data provide compelling evidence that proper differentiation of skeletal stem cells requires *Hox* function but that maintenance of the

skeletal stem cell pool is independent of regional *Hox* function. Despite the demonstration that regional *Hox* expression is maintained throughout the skeleton, it is important to note our results cannot rule out more broadly redundant roles for *Hox* genes that are not addressed by paralogous deletion.

Herein, we show that *Hox* gene function in the skeleton is not restricted to development and that *Hox* genes play a crucial, functional role in adult bone homeostasis. Adult *Hox11* loss of function leads to a replacement of the lamellar cortical bone with an abnormal woven bone-like matrix. We have demonstrated strong evidence that this woven bone matrix is directly produced by the *Hox11* conditional mutant cells and that the woven bone matrix is associated with the defective differentiation and maturation of osteoblasts resulting from the loss of function of *Hox11* in skeletal stem cells.

Whether other *Hox* paralogous genes function to maintain the adult skeleton remains an intriguing question for future studies. Previous studies from our laboratory showing the preservation of region-specific *Hox* expression specifically within progenitor-enriched stem cell populations at adult stages support this likelihood (9). While embryonic loss of function has clearly established that *Hox* genes impart region-specific function that differentially controls skeletal patterning and morphology, results from this study raise the question of whether differential *Hox* gene function continues to be conveyed in a region-specific manner or whether all *Hox* function is similar once the skeleton has been established.

Materials and Methods

Mice. All mice were maintained in a C57BL/6 background. Both male and female mice were used for all experiments. The mouse models *Hoxa11-eGFP* (6) and *Hoxa11-CreERT2* (8) have been previously described. The ROSA26-CAG-loxP-stop-loxP-tdTomato (JAX stock no. 007909) and ROSA26-CreERT2 (JAX stock no. 008463) were purchased from The Jackson Laboratory. The *Hoxd11*-floxed animals were obtained by breeding founder *Hoxd11*-floxed animals to WT C57BL/6 animals for five generations, followed by breeding *Hoxd11*-loxP heterozygotes to each other to produce *Hoxd11*-floxed animals. These animals were periodically bred to WT C57BL/6 animals to avoid genetic drift. The *Col2.3-GFP* mice (36) (kindly provided by Noriaki Ono, University of Michigan, Ann Arbor, Michigan) were then bred with our *Hoxa11* and *Hoxd11* mice to generate animals of appropriate genotype. All animal experiments described in this article were reviewed and approved by the University of Michigan's Committee on Use and Care of Animals, protocol PRO00008674 (to D.M.W.).

Generation of *Hoxd11* Conditional Allele. The *Hoxd11* conditional allele was generated in two injection rounds, targeting each loxP site sequentially. Two guide sequences were targeted to regions of low conservation within the *Hoxd11* intron (5′, upstream) and downstream of the 3′ untranslated region (UTR) (3′, downstream) flanking exon 2 of the *Hoxd11* locus and were cloned into the pT7-Guide Vector (Blue Heron Biotech, LLC). The guide sequence, approximate locations and corresponding protospacer adjacent motif (PAM) sequences are indicated in Fig. 2*A*. Donor oligos contained 60 bp of flanking homology sequence, the loxP sequence (bold letters), and a unique restriction site (EcoRI [5′ loxP] or NheI [3′ loxP], capital letters) for optional use in confirming accurate targeting. Single-stranded DNA oligos were purchased from Integrated DNA Technologies. The 5′ loxP donor oligo sequence (from 5′ to 3′) is as follows: gttgatgagtgggaacacgagagcctcctgcctttcagggagagggtaagtgatctgcc GAATTC ataacttcgtataatgtatgctatacgaagttat gcactggacttaaccccaacctctggctg gcgctcagctcggagttgagcagatgctcctg. The 3′ loxP donor oligo sequence (from 5′ to 3′) is as follows: tctgattagacttacatcatctctagcatttgaaagcaatttgccaccctgctaaataa GCTAGC ataacttcgtataatgtatgctatacgaagttat acgctggcactttataaaatatagaa caaagtaaaatatagttatattgtttcgtaaac.

The guide RNAs were in vitro transcribed from the pT7-Guide Vector using the MEGAshortscript T7 kit (AM1354; Life Technologies), and products were subsequently purified using the MEGAclear kit (AM1908; Life Technologies). Using the pT7-Cas9-Nuclease vector (gift from Moises Mallo, Instituto Gulbenkian de Ciencia, Oeiras, Portugal), the Cas9 messenger RNA (mRNA) was in vitro transcribed using the mMESSAGE mMACHINE T7 ULTRA kit (AMB13455; Life Technologies) and purified using the MEGAclear kit (AM1908; Life Technologies).

Zygote injections were performed as previously described with minor modifications (14). C57BL/6 and SJL mixed background female mice were superovulated and mated with C57BL/6 and SJL mixed background male mice, and one-cell stage embryos were collected for microinjection. CRISPR reagents were microinjected at the following concentrations: Cas9 mRNA (100 ng/μL), single guide RNA (sgRNA) (50 ng/μL), and DNA oligo (50 ng/μL). Injected zygotes were transferred into pseudopregnant females, and resulting progeny were initially screened for potential recombination events via PCR.

The intronic loxP site was targeted first. PCR primers 5′-ATGAGTGGGAACACGAGAGC-3′ and 5′-AGGCTGGCACTGAGATAGGA-3′ were used to screen for loxP insertion. PCR products were cloned for sequencing using the TOPO TA cloning kit (450071; Thermo Fisher). Male mice validated to contain correctly targeted loxP sequence from the first round of injection were used as stud males for targeting of the 3′ region of *Hoxd11* exon 2. PCR primers 5′-AAAGCAATTTGCCACCCTGC-3′ and 5′-ACAGGTAAACCAATGCCCAGA-3′ were used to screen for loxP insertion at the 3′ region of the *Hoxd11* exon 2. Targeting was verified by PCR and sequencing as above. Animals (male or female) confirmed to contain two correctly targeted loxP sites were mated to WT Bl6 animals, and genotyping analyses of the resulting progeny using the PCR primers indicated above were used to screen for germline transmission and the presence of both loxP sites in *cis* along the chromosome.

Tamoxifen Treatment. Mice were fed on tamoxifen chow (TD. 130860; Envigo) at 8 to 10 wk of age for a duration of 3 wk. Based on approximate daily food intake of 4 g per mouse (37) and body weight of 20 to 25 g, mice consumed a concentration of 40 mg/kg tamoxifen per day. The chow was replaced weekly. Both control and conditional mutants were fed on tamoxifen chow.

Bone Tissue Preparations. Mice were killed, and both forelimb zeugopod skeletons were collected by dissecting off the soft tissue, taking care not to disturb the periosteum. All bones were then fixed shaking in 4% paraformaldehyde (PFA) for 2 d at 4 °C and then scanned for microCT if required. Specimens for frozen sections were decalcified in 14% ethylenediaminetetraacetic acid (EDTA) for 7 d and equilibrated in 30% sucrose overnight prior to embedding in OCT media. Cryosections were collected at 10 to 12 μm using the Kawamoto tape method (38). Specimens for paraffin sections were decalcified in 14% EDTA for 7 d and dehydrated in 70% ethanol prior to overnight paraffin processing. Paraffin sections were collected at 5 μm.

Histology, Immunohistochemistry, and Histomorphometry. For all experiments presented, four to eight animals from each genotype were examined. Sample size was determined based on previous literature and our previous experiments. Feasible generation of experimental animals was considered. As *Hox11* expression within the zeugopod skeleton is higher in the ulna compared to the radius, all detailed analyses were carried out in the ulna. Histological stains were performed using standard methods (39). Paraffin sections were deparaffinized and rehydrated by incubating in xylene, followed by a series of washes in decreasing ethanol content (100%, 95%, 70%, ddH_2O). Hematoxylin/eosin (H&E) stains were processed as previously reported (39). Tartrate-resistant acidic phosphatase (TRAP) staining (387A-1KT; Sigma-Aldrich) and picrosirius red stain (ab150681; Abcam) were performed according to the manufacturer's protocol. For the visualization of the osteocyte lacunocanalicular network, the bone sections were processed as previously reported with minor modifications (40). All histological images were acquired on an Eclipse E800 microscope (Nikon).

For immunostaining, cryosections were blocked with 5% donkey serum and incubated with primary antibodies overnight at 4 °C against osterix (ab22552, 1: 300; Abcam), osteopontin (AF808, 1:200; R&D Systems), and osteocalcin (DS-PB-01521, 1:200, antibody no longer commercially available; RayBiotech). Secondary antibodies were incubated at room temperature for 1 h: donkey-anti-rabbit–Alexa Fluor 647 (A31573, 1:500; Thermo Fisher) and donkey-anti-goat–Alexa Fluor 488 (A11055, 1:500; Thermo Fisher). SOST was visualized using a modified signal amplification protocol. Sections were incubated in SOST (AF1589, 1:100; R&D Systems) overnight at 4 °C followed by donkey-anti-goat–biotin secondary (705-067-003, 1:400; Jackson ImmunoResearch). The biotinylated secondary was detected using the Vectastain Elite ABC kit (PK-6100; Vector Laboratories), and the signal was amplified by Alexa Fluor 488 Tyramide reagent (B40853; Thermo Fisher). Endogenous Hoxa11eGFP fluorescence was quenched after the decalcification process and was visualized using chicken-anti-GFP (ab13970, 1:1,000; Abcam) and donkey-anti-chicken–Alexa Fluor 488 (A11039, 1:500; Invitrogen). All fluorescent images were acquired on a Leica Upright SP5x two-photon confocal microscope. Confocal z-stacks were captured through entire sections at a thickness of 1 to 2 μm, and images were stacked using Photoshop. Large images were stitched (when necessary) using Photoshop.

Fluorophore-labeled CMP and CI were synthesized as described previously (20). Briefly, ^{Cy5}CMP has the sequence: Cy5-Gly-$(SerGly)_2$-$(flpHypGly)_7$-OH, where flp refers to (2*S*,4*S*)-4-fluoroproline and Hyp refers to (2*S*,4*R*)-4-hydroxyproline. ^{Cy5}CI has the sequence: Cy5-Gly-$(SerGly)_2$-$(HypFlpGly)_7$-OH. Paraffin bone sections were stained in the dark for 1 h at room temperature and then washed with 1× phosphate-buffered saline (PBS) followed by imaging.

Data Availability Statement. All data are available in the main text and *SI Appendix*.

ACKNOWLEDGMENTS. We thank Chris Stephan for technical assistance in microCT scanning of the bone specimens. We also thank Drs. Ernestina Schipani, Karl Jepsen, and Kenneth Kozloff for their input and advice on experiments. We acknowledge the help and service provided by the Orthopedic Research Laboratory (ORL) staff. We acknowledge the help and service of the Transgenic Animal Model Core of the University of Michigan's Biomedical Research Core Facilities. Research reported in this publication was mainly supported by National Institute of Arthritis and Musculoskeletal and Skin Diseases of the National Institutes of Health (NIH) Award R01 AR061402 (to D.M.W.). Support was also provided by Michigan Integrative Musculoskeletal Health Core Center Award P30 AR069620, by training awards granted by the National Institute of Dental and Craniofacial Research of the NIH under Award T32 DE007057 (to K.M.P. and J.Y.S.), by the National Institute of Child Health and Human Development of the NIH under Award T32 HD007505 (to K.M.P.), a Warner-Lambert Fellowship from the University of Michigan Cellular and Molecular Biology training program (to J.Y.S.), and National Institute of Arthritis and Musculoskeletal and Skin Diseases of the NIH Award R56 AR044276 (to R.T.R.). D.M.W. and R.T.R. would like to dedicate this manuscript to Dr. Hector F. DeLuca (former PhD mentor and former chair of Biochemistry at University of Wisconsin-Madison, respectively) on the occasion of his 90th birthday.

1. M. Mallo, D. M. Wellik, J. Deschamps, Hox genes and regional patterning of the vertebrate body plan. *Dev. Biol.* **344**, 7–15 (2010).
2. C. Fromental-Ramain *et al*., Specific and redundant functions of the paralogous Hoxa-9 and Hoxd-9 genes in forelimb and axial skeleton patterning. *Development* **122**, 461–472 (1996).
3. C. Fromental-Ramain *et al*., Hoxa-13 and Hoxd-13 play a crucial role in the patterning of the limb autopod. *Development* **122**, 2997–3011 (1996).
4. D. M. Wellik, M. R. Capecchi, Hox10 and Hox11 genes are required to globally pattern the mammalian skeleton. *Science* **301**, 363–367 (2003).
5. A. P. Davis, D. P. Witte, H. M. Hsieh-Li, S. S. Potter, M. R. Capecchi, Absence of radius and ulna in mice lacking hoxa-11 and hoxd-11. *Nature* **375**, 791–795 (1995).
6. L. T. Nelson, S. Rakshit, H. Sun, D. M. Wellik, Generation and expression of a Hoxa11eGFP targeted allele in mice. *Dev. Dyn.* **237**, 3410–3416 (2008).
7. I. T. Swinehart, A. J. Schlientz, C. A. Quintanilla, D. P. Mortlock, D. M. Wellik, Hox11 genes are required for regional patterning and integration of muscle, tendon and bone. *Development* **140**, 4574–4582 (2013).
8. K. M. Pineault *et al*., Hox11 genes regulate postnatal longitudinal bone growth and growth plate proliferation. *Biol. Open* **4**, 1538–1548 (2015).
9. D. R. Rux *et al*., Regionally restricted Hox function in adult bone marrow multipotent mesenchymal stem/stromal cells. *Dev. Cell* **39**, 653–666 (2016).
10. D. R. Rux *et al*., Hox11 function is required for region-specific fracture repair. *J. Bone Miner. Res.* **32**, 1750–1760 (2017).
11. K. M. Pineault, J. Y. Song, K. M. Kozloff, D. Lucas, D. M. Wellik, Hox11 expressing regional skeletal stem cells are progenitors for osteoblasts, chondrocytes and adipocytes throughout life. *Nat. Commun.* **10**, 3168 (2019).
12. P. Leucht *et al*., Embryonic origin and Hox status determine progenitor cell fate during adult bone regeneration. *Development* **135**, 2845–2854 (2008).
13. K. B. Ackema, J. Charité, Mesenchymal stem cells from different organs are characterized by distinct topographic Hox codes. *Stem Cells Dev.* **17**, 979–991 (2008).
14. Y. Wu *et al*., Correction of a genetic disease in mouse via use of CRISPR-Cas9. *Cell Stem Cell* **13**, 659–662 (2013).
15. C. J. Hernandez, R. J. Majeska, M. B. Schaffler, Osteocyte density in woven bone. *Bone* **35**, 1095–1099 (2004).
16. M. D. McKee, W. G. Cole, "Bone matrix and mineralization" in *Pediatric Bone*, F. Glorieux, J. Pettifor, H. Juppner, Eds. (Elsevier Inc., 2012), chap. 2.
17. R. F. M. van Oers, H. Wang, R. G. Bacabac, Osteocyte shape and mechanical loading. *Curr. Osteoporos. Rep.* **13**, 61–66 (2015).
18. R. Lattouf *et al*., Picrosirius red staining: A useful tool to appraise collagen networks in normal and pathological tissues. *J. Histochem. Cytochem.* **62**, 751–758 (2014).
19. L. C. U. Junqueira, G. Bignolas, R. R. Brentani, Picrosirius staining plus polarization microscopy, a specific method for collagen detection in tissue sections. *Histochem. J.* **11**, 447–455 (1979).
20. J. M. Dones *et al*., Optimization of interstrand interactions enables burn detection with a collagen-mimetic peptide. *Org. Biomol. Chem.* **17**, 9906–9912 (2019).
21. J. Ljusberg *et al*., Proteolytic excision of a repressive loop domain in tartrate-resistant acid phosphatase by cathepsin K in osteoclasts. *J. Biol. Chem.* **280**, 28370–28381 (2005).
22. M. J. F. Blumer *et al*., Role of tartrate-resistant acid phosphatase (TRAP) in long bone development. *Mech. Dev.* **129**, 162–176 (2012).
23. P. Gradin, K. Hollberg, A. I. Cassady, P. Lång, G. Andersson, Transgenic overexpression of tartrate-resistant acid phosphatase is associated with induction of osteoblast gene expression and increased cortical bone mineral content and density. *Cells Tissues Organs (Print)* **196**, 68–81 (2012).
24. A. Rutkovskiy, K.-O. Stensløkken, I. J. Vaage, Osteoblast differentiation at a glance. *Med. Sci. Monit. Basic Res.* **22**, 95–106 (2016).
25. J. B. Lian, G. S. Stein, "Osteoblast biology" in *Osteoporosis*, R. Marcus, D. Feldman, D. Nelson, C. Rosen, Eds. (Elsevier Inc., 2008), chap. 6.
26. J. Klein-Nulend, R. G. Bacabac, M. G. Mullender, Mechanobiology of bone tissue. *Pathol. Biol. (Paris)* **53**, 576–580 (2005).
27. F. M. Pavalko *et al*., A model for mechanotransduction in bone cells: The load-bearing mechanosomes. *J. Cell. Biochem.* **88**, 104–112 (2003).
28. L. F. Bonewald, Generation and function of osteocyte dendritic processes. *J. Musculoskelet. Neuronal Interact.* **5**, 321–324 (2005).
29. C. H. Turner, A. G. Robling, R. L. Duncan, D. B. Burr, Do bone cells behave like a neuronal network? *Calcif. Tissue Int.* **70**, 435–442 (2002).
30. A. Lindahl *et al*., "Cartilage and Bone Regeneration" in *Tissue Engineering*, C. A. V. Blitterswijk, J. De Boer, Eds. (Elsevier Inc., ed. 2, 2014).
31. N. Reznikov, R. Shahar, S. Weiner, Bone hierarchical structure in three dimensions. *Acta Biomater.* **10**, 3815–3826 (2014).
32. F. Shapiro, J. Y. Wu, Woven bone overview: Structural classification based on its integral role in developmental, repair and pathological bone formation throughout vertebrate groups. *Eur. Cell. Mater.* **38**, 137–167 (2019).
33. S. Gross, Y. Krause, M. Wuelling, A. Vortkamp, Hoxa11 and Hoxd11 regulate chondrocyte differentiation upstream of Runx2 and Shox2 in mice. *PLoS One* **7**, e43553 (2012).
34. W. Zhao, M. H. Byrne, Y. Wang, S. M. Krane, Osteocyte and osteoblast apoptosis and excessive bone deposition accompany failure of collagenase cleavage of collagen. *J. Clin. Invest.* **106**, 941–949 (2000).
35. V. Bradaschia-Correa *et al*., Hox gene expression determines cell fate of adult periosteal stem/progenitor cells. *Sci. Rep.* **9**, 5043 (2019).
36. Z. Kalajzic *et al*., Directing the expression of a green fluorescent protein transgene in differentiated osteoblasts: Comparison between rat type I collagen and rat osteocalcin promoters. *Bone* **31**, 654–660 (2002).
37. A. A. Bachmanov, D. R. Reed, G. K. Beauchamp, M. G. Tordoff, Food intake, water intake, and drinking spout side preference of 28 mouse strains. *Behav. Genet.* **32**, 435–443 (2002).
38. T. Kawamoto, M. Shimizu, A method for preparing 2- to 50-micron-thick fresh-frozen sections of large samples and undecalcified hard tissues. *Histochem. Cell Biol.* **113**, 331–339 (2000).
39. L. Mangiavini, C. Merceron, E. Schipani, Analysis of mouse growth plate development. *Curr. Protoc. Mouse Biol.* **6**, 67–130 (2016).
40. E. J. Jáuregui *et al*., Parallel mechanisms suppress cochlear bone remodeling to protect hearing. *Bone* **89**, 7–15 (2016).